CHIN. PHYS. LETT. Vol. 37, No. 1 (2020) 018101

Fast Liquid Phase Epitaxial Growth for Perovskite Single Crystals *

Yu-Wei Li(李雨巍), Xin Wang(王昕)**, Guan-Wen Li(李冠文), Yao Wu(吴瑶), Yu-Zhu Pan(潘禹竹), Yu-Bing Xu(徐玉冰), Jing Chen(陈静), Wei Lei(雷威)**

Joint International Research Laboratory of Information Display and Visualization, School of Electronic Science and Engineering, Southeast University, Nanjing 210096

(Received 19 September 2019)

Semiconductors grown by the solution-processed method have shown low-cost, facile fabrication process and comparable performance. However, there are many reasons why it is difficult to achieve high quality films. For example, lattice constant mismatch is one of the problems when photovoltaic devices made of organ metallic perovskites. In this work, $MAPbBr_3$ ($MA = CH_3NH_3^+$) perovskites single crystals grown on the surface of $MAPbBr_{2.5}Cl_{0.5}$ perovskites single crystals via liquid epitaxial growth method is demonstrated. It is found that when the lattice constants of the two perovskite single crystals are matched, another crystal can be grown on the surface of one crystal by epitaxial growth. The whole epitaxy growth process does not require high heating temperature and long heating time. X-ray diffraction method is used to prove the lattice plane of the substrate and the epitaxial grown layer. A scanning electron microscope is used to measure the thickness of the epitaxial layer. Compared with perovskite-based photodetectors without epitaxial growth layer, perovskite-based photodetectors with epitaxial growth layer have lower dark current density and higher optical responsibility.

PACS: 81.10.−h, 81.15.−z, 73.40.Lq DOI: 10.1088/0256-307X/37/1/018101

In the past few years, organo-lead halide perovskites $MAPbX_3$ (MA=$CH_3NH_3^+$, X = Cl^-, Br^- or I^-) have attracted a great deal of attention from scientists and have become a research focus, thanks to their excellent optical and electrical properties, together with their inexpensive and low-temperature solution process ability.[1−4] So far, there are countless reports on applications of these materials in high efficiency solar cells, light emitting diodes, lasers and photodetectors.[4−9] In order to realize these exciting photovoltaic devices, heterojunctions are always necessary to establish specific band gap structure for better performances.[10] However, based on perovskites' physical and chemical properties, mismatching lattice materials such as electron transport layers (ETL) including layers of C_{60} and bathocuproine (BCP) and hole transport layers (HTL) including poly[N, N'-bis(4-butylphenyl)-N, N'-bis(phenyl)benzidine] (poly-TPD), poly(3,4-ethylenedioxythiophene)/poly(styrene sulfonate) (PEDOT:PSS) and poly(9-vinylcarbazole) (PVK) sandwich perovskites through spin-coating, evaporation deposit and plating.[11−14] As a result, unexpected noise and instability from inhomogeneous thickness, rough surface and high defect density restrict the performance of perovskites-based photovoltaic devices.[15−17]

To solve this problem, fast liquid epitaxial growth (FLPE) is investigated here to grow perovskites with different halide ratios.[16,18−22] $MAPbBr_{2.5}Cl_{0.5}$ and $MAPbBr_3$ perovskite single crystals (PSCs) are chosen to be the substrate and the epitaxial layer, respectively, due to their same cubic structure, nearly lattice constant and similar growth condition.[23−25] A high-quality $MAPbBr_{2.5}Cl_{0.5}$ is synthesized from inverse temperature crystallization as previously reported, and epitaxial growth happens in saturated $MAPbBr_3$ PSC precursor. The boundary between two layers and the photo-electron property are investigated. This work provides useful information to grow high performance perovskites-based devices and give a better path to investigate the crystallization process of perovskites.

Transparent and cubic $MAPbBr_{2.5}Cl_{0.5}$ perovskites single crystals (PSCs) are obtained by inverse temperature crystallization of mixed solutions. Firstly, $MAPbBr_{2.5}Cl_{0.5}$ PSCs are placed in the precursor solution for growth of the $MAPbBr_3$ PSCs. Secondly, the precursor solution is heated to 65℃ on the heating stage (IKA C-MAG HS7) for 7 min. When the surface color of the $MAPbBr_{2.5}Cl_{0.5}$ PSCs changes, the heating is stopped and the PSCs are removed from the precursor solution.

The energy dispersive x-ray (EDX) spectra are investigated by X'TRA. The cross section and top face of the hetero PSC are identified by a scanning electron microscope (SEM, Quanta 200 FEI).

The bottom face of the crystal is polished by the abrasive until the $MAPbBr_3$ PSC is removed. The structure Au/$MAPbBr_3$ PSC/$MAPbBr_{2.5}Cl_{0.5}$ PSC/Ag is used to measure the resistivity. Au and Ag are deposited by thermal evaporation (ZZS500-3/G). A Keithley 2400 is used as dc power and amperometer.

Figure 1(a) shows the process of the fast liquid phase epitaxial growth of $MAPbBr_3$ on the $MAPbBr_{2.5}Cl_{0.5}$ PSC. To determine the crystal quality of the $MAPbBr_3$ grown on $MAPbBr_{2.5}Cl_{0.5}$ PSC, x-ray diffraction (XRD) characterization is per-

*Supported by the National Key R&D Program of China (Grant Nos. 2017YFC0111500 and 2016YFB0401600), the National Natural Science Foundation Project (Grant Nos. 61775034, 61571124, and 61674029), International Cooperation Program of Jiangsu Province (Grant No. BZ2018056), and the NSFC Research Fund for International Young Scientists (Grant No. 61750110537).

**Corresponding author. Email: 230159424@seu.edu.cn; lw@seu.edu.cn

© 2020 Chinese Physical Society and IOP Publishing Ltd

formed. XRD patterns are obtained to characterize the crystallinity of MAPbBr$_3$ on MAPbBr$_{2.5}$Cl$_{0.5}$ PSC, MAPbBr$_{2.5}$Cl$_{0.5}$ PSC and MAPbBr$_3$ PSC, as shown in Figs. 1(b) and 2(c). It is obvious that the diffraction angle of the peaks of these three PSCs are very similar. It is found that the strongest peaks of the epitaxy growth for MAPbBr$_3$ are observed at $2\theta =$ 16.7°, 31°, 47° and 62.5°, while the strongest peaks of the MAPbBr$_3$ PSC and MAPbBr$_{2.5}$Cl$_{0.5}$ PSC are observed at $2\theta = 16°$, 30°, 46°, 62° and $2\theta = 18°$, 32.5°, 48°, 65°. Similarly, they all belong to (100) planes. In particular, each strong peak can be divided into K_α and K_β, which are characteristic lines of copper that indicate high-quality crystallization. The lattice constants of three kinds of crystals can also be calculated from the XRD results. The lattice constants of single MAPbBr$_3$ PSC and the epitaxial growth MAPbBr$_3$ PSC are 5.87185 Å and 5.86355 Å, while the lattice constant of MAPbBr$_{2.5}$Cl$_{0.5}$ PSC is calculated to be 5.79930 Å. According to the equation of lattice mismatch (mismatch rate $= (a_1 - a_2)/(a_1 + a_2)$) we work out that the lattice mismatch of the MAPbBr$_3$ PSC and the MAPbBr$_{2.5}$Cl$_{0.5}$ PSC is 0.55%, which is below 1%, indicating that their lattice is matched.

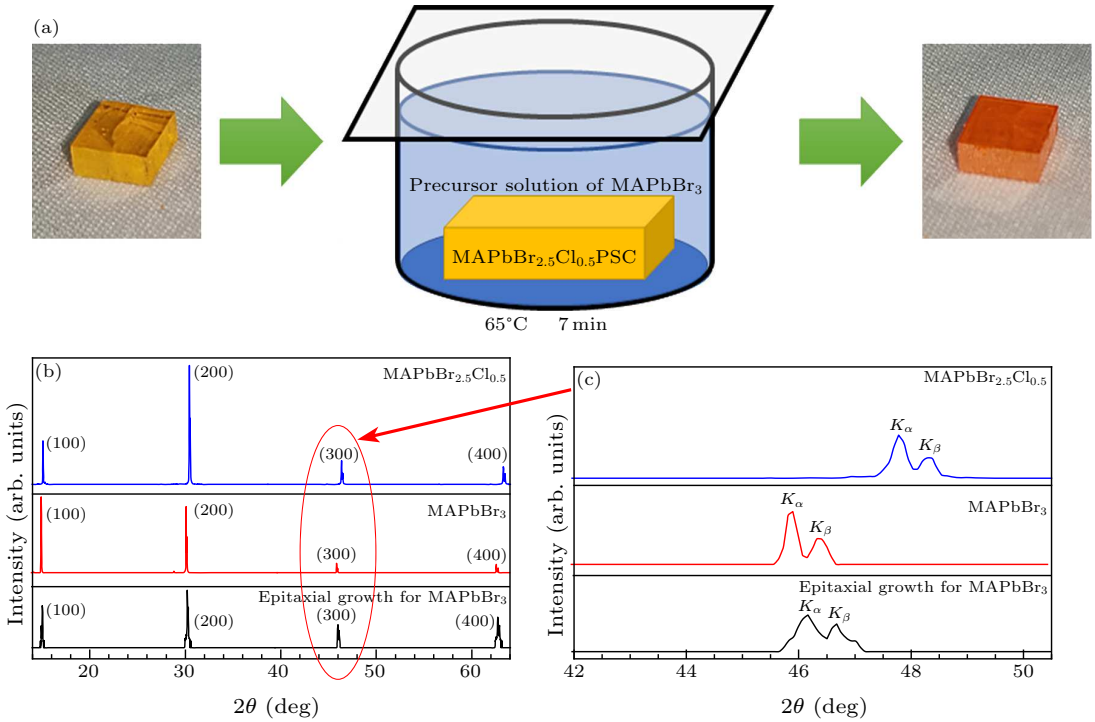

Fig. 1. (a) Illustration of the fast liquid phase epitaxial growth, (b) long-range x-ray diffraction results of the $CH_3NH_3PbCl_{0.5}Br_{2.5}$ PSC, epitaxy growth for $CH_3NH_3PbBr_3$ and the $CH_3NH_3PbBr_3$ PSC, (c) XRD results from 42° to 50° of former three kinds of PSCs.

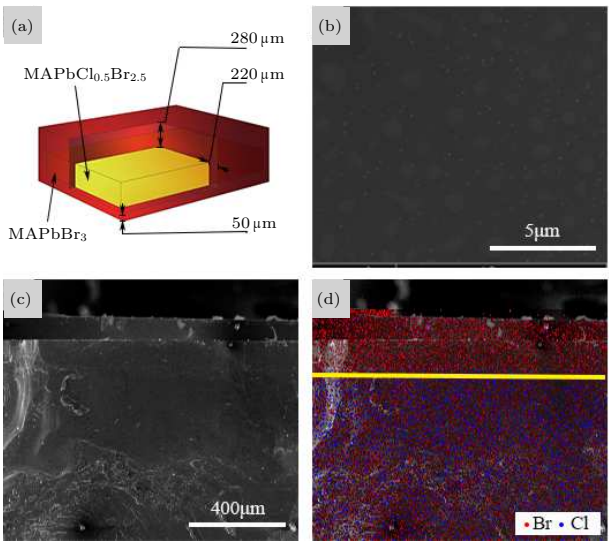

Fig. 2. (a) Structural charts of crystals grown by epitaxy, (b) SEM images of the top face of FLPE PSC, (c) SEM images of the section of FLPE PSC, (d) EDX of element distribution in section.

After proving that the MAPbBr$_3$ PSC is epitaxially grown on the surface of the MAPbBr$_{2.5}$Cl$_{0.5}$ PSC, the structure of the whole hetero crystal needs to be explored as illustrated in Fig. 2(a). Figure 2(b) shows the SEM image of the top face of the crystal. There are no cracks on the top face of the crystal, which also indicates uniform and flat surface. The boundary between MAPbBr$_{2.5}$Cl$_{0.5}$ PSC and MAPbBr$_3$ PSC is found, and the thickness of MAPbBr$_3$ PSC can also be measured by analyzing the SEM image of the cross section and the results of energy dispersive x-ray spectroscopy (EDX) for the cross section which are shown in Figs. 2(c) and 2(d). In Fig. 2(d), red and blue represent bromine and chlorine, respectively. The bromine distributes above the yellow line while the chlorine and the bromine distribute below the yellow line, which indicates that the yellow line is the boundary between MAPbBr$_3$ PSC and MAPbBr$_{2.5}$Cl$_{0.5}$ PSC. Based on the results from x-ray, SEM and EDX, the possible structure of the crystal is shown in Fig. 2(a), where the red region represents epitaxial growth for

the MAPbBr$_3$ PSC and the yellow region represents the MAPbBr$_{2.5}$Cl$_{0.5}$ PSC as the core and substrate. The thicknesses of the top face epitaxy layer, the surrounding epitaxy layer and the bottom face epitaxy layer are 280 μm, 220 μm and 50 μm. In the process of crystal growth, the ability of accepting atoms along different crystal directions is different, that is to say, it can grow preferentially in some crystal directions. This leads to the fact that the thickness of the grown perovskite single crystals is different on different faces of the substrate due to the solution supersaturation distribution.

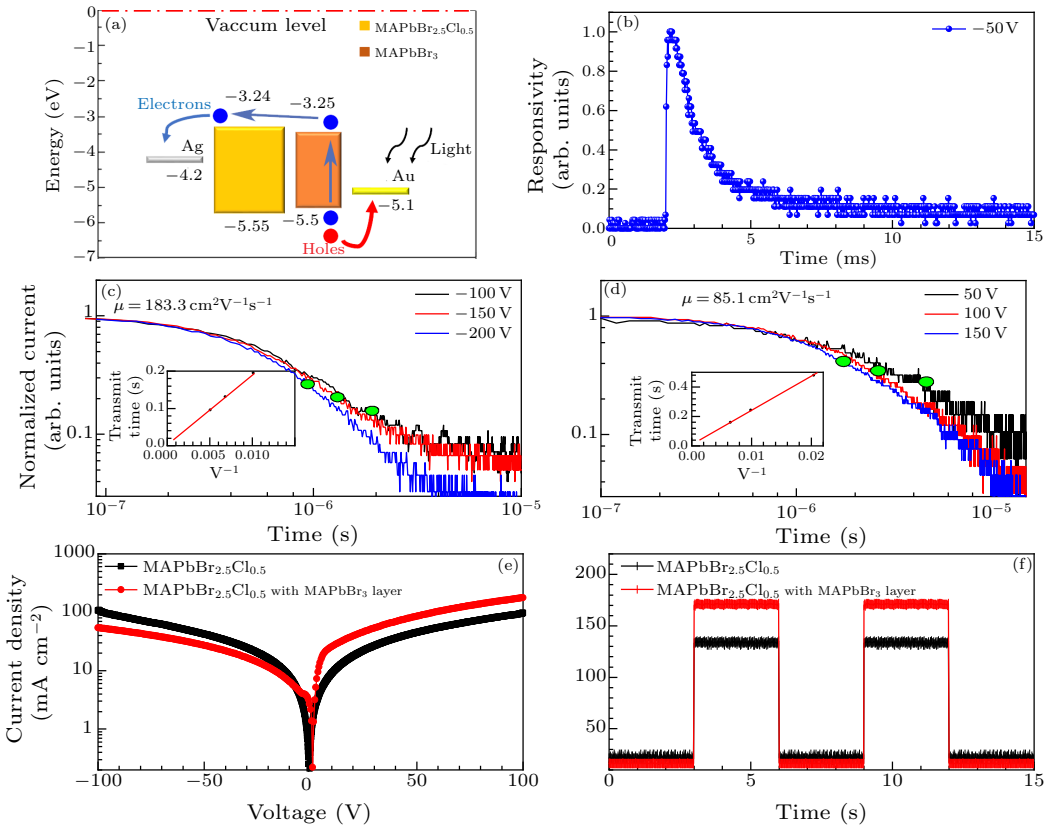

Fig. 3. (a) Band structure of the whole detector, (b) response time, (c) average electron mobility, (d) average hole mobility, (e) current density–voltage (I–V) curves of the photodetectors in dark state, (f) photocurrent density of the photodetector light illumination at voltages bias −30 V.

One side of MAPbBr$_{2.5}$Cl$_{0.5}$ PSC is exposed from the cover of MAPbBr$_3$ PSC by cutting and polishing. Then silver and Au are evaporated on the opposite faces of the hetero PSC as cathode and anode to realize a photodetector. The band structure of the photodetector is shown in Fig. 3(a). When negative bias is applied between the electrodes, a pulsed laser with a wavelength of 355 nm is incident into the anode. The holes generated near the anode are absorbed rapidly, and electrons pass through the whole crystal to the cathode under the action of electric field. At the voltage bias −50 V, the rise time and the fall time are about 140 ns and 7.2 μs, as shown in Fig. 3(b). In Figs. 3(c) and 3(d), the average electron mobility is 183.3 cm^2·V^{-1}s^{-1} and the average hole mobility is 85.1 cm^2·V^{-1}s^{-1} for the MAPbBr$_{2.5}$Cl$_{0.5}$ PSC with epitaxy layer measured by the time-of-flight method (TOF method). It can be clearly observed from Figs. 3(e) and 3(f) that the current density of devices with epitaxy layer is less than that of devices without epitaxy layer in darkness, and the light response current density of devices with the epitaxy layer is also larger than that of devices without the epitaxy layer at voltages bias −30 V. Due to the formation of heterojunctions in the inner layer MAPbBr$_{2.5}$Cl$_{0.5}$ PSC and the epitaxial layer MAPbBr$_3$ PSC. Compared with the spin coating with mismatched lattice, the heterojunction surface has good crystal characteristics. Less surface defects significantly reduce dark current noise. At the same time, the heterostructure can improve the bandwidth and increase the responsivity. The dark current density decreases by 20 μA/cm^2 and the photocurrent density increases by 90 μA/cm^2 at voltages bias −30 V with periodic white light illumination. The optical power density of white light illumination used in our experiment is 120 μW/cm^2, the responsibility of the photo-detection experiments is 0.58 A/W at voltages bias −30 V by $R = (I_{\text{light}} - I_{\text{dark}})/P_{\text{optical}}$.

In summary, epitaxy growth of the MAPbBr$_3$ PSC on the lattice-matched surface of the MAPbBr$_{2.5}$Cl$_{0.5}$ PSC which is dipped into the precursor of MAPbBr$_3$ under the heating condition of 65℃ for 7 min. The speed of the growth process is controllable. When it is at the crystal growth temperature, the growth speed

is highly related to the evaporation speed of the precursor. The results show that liquid phase epitaxy growth is suitable for lattice-matched perovskite single crystals. When the two kinds of crystal lattices do not match, we can look for a third kind of crystal which matches the two kinds of crystal lattice as a buffer. The growth of perovskite single crystal heterojunction by FLPE can realize the combination of new materials and mature semiconductor technology. The photodetectors that are fabricated from the epitaxially grown crystals have heterojunction characteristics and have dark current lower than the photodetectors fabricated from non-epitaxially grown crystals at the same bias voltage. These results provide some valuable information for fabrication of devices made of perovskites/PSC.

References

[1] Wang X et al 2018 *Phys. Status Solidi RRL* **12** 1800380
[2] Kim Y C, Kim K H, Son D, Jeong D, Seo J, Choi Y S, Han I T, Lee S Y and Park N 2017 *Nature* **550** 87
[3] Wei W et al 2017 *Nat. Photon.* **11** 315
[4] Berry J et al 2015 *Adv. Mater.* **27** 5102
[5] Rong Y G, Liu L F, Mei A Y, Li X and Han H W 2015 *Adv. Energy Mater.* **5** 1501066
[6] Dou L, Yang Y M, You J, Hong Z, Chang W, Li G and Yang Y 2014 *Nat. Commun.* **5** 5404
[7] Kazim S, Nazeeruddin M K, Gräetzel M and Ahmad S 2014 *Angew. Chem. Int. Ed.* **53** 2812
[8] An T, Tu C and Gong W 2018 *Acta Phys. Sin* **67** 198503 (in Chinese)
[9] Zhang J X, Guo H X, Pan X Y et al 2018 *Chin. Phys. B* **27** 108501
[10] Wu C Y, Gu J H, Feng Y Y, Xue Y and Lu J X 2012 *Acta Phys. Sin* **61** 157803 (in Chinese)
[11] Liang G X, Fan P, Luo J, Gu D and Zheng Z 2015 *Prog. Photon.* **23** 1901
[12] Fan P, Gu D, Liang G, Luo J, Chen J, Zheng Z and Zhang D 2016 *Sci. Rep.* **6** 29910
[13] Li X Y, Zhao L, Wei X Y, Li H and Jin K X 2018 *Chin. Phys. B* **27** 117501
[14] Xiao S et al 2018 *Chin. Phys. B* **27** 078801
[15] Kim H, Im S H and Park N 2014 *J. Phys. Chem. C* **118** 5615
[16] Zhu P C et al 2016 *Nano Lett.* **16** 871
[17] Dong R et al 2015 *Adv. Mater.* **27** 1912
[18] Ji L, Hsu H, Lee J C, Bard A J and Yu E T 2018 *Nano Lett.* **18** 994
[19] Chen J, Fu Y, Samad L, Dang L, Zhao Y, Shen S, Guo L and Jin S 2017 *Nano Lett.* **17** 460
[20] Wei H, DeSantis D, Wei W, Deng Y, Guo D, Savenije T J, Cao L and Huang J 2017 *Nat. Mater.* **16** 826
[21] Fang Y, Dong Q, Shao Y, Yuan Y and Huang J 2015 *Nat. Photon.* **9** 679
[22] Li F, Ma C, Wang H, Hu W, Yu W, Sheikh A D and Wu T 2015 *Nat. Commun.* **6** 8238
[23] Wang X, Wu Y, Li G, Wu J, Zhang X, Li Q, Wang B, Chen J and Lei W 2018 *Adv. Electron. Mater.* **4** 1800237
[24] Jiang S G et al 2019 *Mater. Lett.* **236** 26
[25] Xiao R, Hou Y, Fu Y, Peng X, Wang Q, Gonzalez E, Jin S and Yu D 2016 *Nano Lett.* **16** 7710